GEOTECHNICAL SPECIAL PUBLICATION NO. 182

PAVEMENTS AND MATERIALS

CHARACTERIZATION, MODELING, AND SIMULATION

PROCEEDINGS OF SYMPOSIUM ON PAVEMENT MECHANICS AND MATERIALS AT THE 18TH ASCE ENGINEERING MECHANICS DIVISION (EMD) CONFERENCE

June 3-6, 2007
Blacksburg, Virginia

SPONSORED BY
Pavements Committee of The Geo-Institute
American Society of Civil Engineers

Task Committee on Mechanics of Pavements, Inelastic Committee, and Granular Materials Committee of The Engineering Mechanics Institute, American Society of Civil Engineers

EDITED BY
Zhanping You
Ala R. Abbas
Linbing Wang

Published by the American Society of Civil Engineers

REFERENCES

Buttlar, W. G., and Dave, E. V. (2005). "A Micromechanics-Based Approach for Determining Presence and Amount of Recycled Asphalt Pavement Material in Asphalt Concrete (With Discussion)." *2005 Journal of the Association of Asphalt Paving Technologists: From the Proceedings of the Technical Sessions*, 74, 829-884.

Buttlar, W. G., and You, Z. (2001). "Discrete element modeling of asphalt concrete: Microfabric approach." *Transportation Research Record*, 1757, 111-118.

Chang, G. K., and Meegoda, J. N. (1997). "Micromechanical Simulation of Hot Mixture Asphalt." *ASCE J. Engng. Mech.*, 123(5), 495-503.

Melis Maynar, M. J., and Medina Rodriguez, L. E. (2005). "Discrete Numerical Model for Analysis of Earth Pressure Balance Tunnel Excavation." 131, 1234-1242.

Yao, M., and Anandarajah, A. (2003). "Three-dimensional discrete element method of analysis of clays." 129, 585-596.

You, Z., and Buttlar, W. G. (2004). "Discrete Element Modeling to Predict the Modulus of Asphalt Concrete Mixtures." *Journal of Materials in Civil Engineering, ASCE*, 16(2), 140-146.

You, Z., and Buttlar, W. G. (2006). "Micromechanical Modeling Approach to Predict Compressive Dynamic Moduli of Asphalt Mixture Using the Distinct Element Method." *Transportation Research Record: Journal of the Transportation Research Board, National Research Council, Washington, D.C.*, 1970, 73-83.

You, Z., and Dai, Q. (2007). "A Review of Advances in Micromechanical Modeling of Aggregate-Aggregate Interaction in Asphalt Mixture." *Canadian Journal of Civil Engineering* 34(2), 239-252.

Zeghal, M. (2004). "Discrete-element method investigation of the resilient behavior of granular materials." 130, 503-509.

Responses of a Transversely Isotropic Layered Half-Space to Multiple Horizontal Loads

Ewan Y.G. Chen[1] and Ernie Pan[2], M. ASCE

[1]Graduate Student, The Department of Civil Engineering, University of Akron, Akron, OH 44325-3905; yc39@uakron.edu

[2]Associate Professor, The Department of Civil Engineering and The Department of Applied Mathematics, University of Akron, Akron, OH 44325-3905; pan2@uakron.edu

ABSTRACT: In this work, the displacements and stresses at any point in a transversely isotropic layered half-space under multiple horizontal loads are studied. The transversely isotropic plane is assumed to be parallel to the surface plane, and uniformly distributed circular loads with different magnitudes, radii and orientations are applied to the pavement surface. Based on the cylindrical system of vector functions in the transformed domain, the governing equations are first decoupled into two sets of equations related to the *LM*-type and *N*-type respectively. Solutions for the multilayered half-space in the transformed domain are then derived by virtue of the propagator matrix method. Solutions in the physical domain are then expressed in terms of the Bessel function integration. The method of superposition is finally utilized for multiple loads. We remark that while the propagator matrix method has been frequently used to solve the vertical loading problem in layered half-spaces, which only involve the *LM*-type equation, the corresponding horizontal loading problem involving multiple circular loads in a transversely isotropic layered half-space has not been addressed in the literature. A computer program has been coded by the authors' research group and numerical results obtained from this program for the isotropic layered half-space have been verified with existing ones. Further presented in this paper are the results for the transversely isotropic layered half-space, with examples elucidating clearly the effect of material anisotropy on the responses, especially on pavement failure. It is also observed that, in terms of computation, the developed program is very accurate, efficient and flexible. For instance, our program can easily handle more than 10,000 field points with more than 1,000 pavement layers.

INTRODUCTION

The Kelvin solution (e.g., Love 1927) for the concentrated load acting in an infinite solid is well known, and many problems of science and engineering importance can be obtained from this fundamental solution. The classical Boussinesq solution (e.g., Love 1927) dealing with a vertical force applied at the surface of a semi-infinite solid has found a number of practical applications in foundation engineering, pavement engineering, et al. While the Cerruti solution (e.g., Love 1927)) is for the problem of a horizontal force applied at the surface of a half-space, the Mindlin solution (Mindlin, 1936) is to solve the problem with the point load in the interior of the half-space. The Mindlin solution can easily be deduced to the other three classical solutions mentioned above. It should be mentioned that all these classical solutions are for the point load and homogenous material.

By integrating solutions of the concentrated load over the loading domain, solution for the case of a uniformly distributed load within a circle can be arrived. However, this solution cannot be extended to the multi-layered structure. Burmister (1943, 1945) pioneered the analytical solutions using layered elastic theory, first for a two-layered pavement and later for a three-layered pavement. It should be noticed that a lot of research for multi-layered structures are focused on the vertical loads, an extension of the Boussinesq problem, whilst the research for the responses of a layered half-space structure to the horizontal load is usually omitted. For example, in the pavement engineering, the vehicle load acting on the pavement surface is usually modeled as a vertical load, omitting the horizontal load in practice, such as the friction force between the tire of the vehicle and pavement surface.

Among the few studies closely related to horizontal loads, Wang (1983) proposed a method, named recursion and back-substitution, and discussed the solution of layered elasticity under vertical and horizontal loads. Pan (1989a) proposed the special vector function to deal with the problem of isotropic layered half-space structure under single load, either vertically or horizontally. Pan (1989b) then introduced two sets of vector functions in both the cylindrical and Cartesian coordinates and derived the general formalism for the transversely isotropic layered half-space under general loads. It should be mentioned that for the layered structure problem, the solutions are extremely complicated as compared to the classical Boussinesq and Cerruti solutions. Thus only single vertical and horizontal load was considered. Later on, Pan (1997) proposed the static Green's functions in the multilayered transversely isotropic half-space, and displacement and stress fields under vertical and horizontal point load were presented and compared. An independent work was presented by Yue and Yin (1998) dealing with similar problems. Matsui et al. (2002) used Hankle transform and biharmonic function to deal with the problem of layered isotropic half-space structure under multiple horizontal loads, and developed a program named Analysis of Multi-layered Elastic Structure (AMES) based on their method.

The goal of this research is, therefore, to discuss in detail the problem of horizontal loading on a multi-layered pavement surface based on the vector functions introduced by Pan (1989b), and to develop a computer program for analyzing the responses of a multilayered pavement system by the horizontal load. By expressing the governing equations in the cylindrical system of vector functions, the original coupling

equations can be decoupled into two types of equations in terms of the vector functions, and solutions can be obtained in the form of integration of Bessel function, including first kind of zero and first orders. In addition, the propagator matrix method is utilized to deal with the layered half-space structure. The principle of superposition thereafter is adopted for multiple loads, and thus the final solutions for transversely isotropic layered half-space structure to multiple loads are established.

A computer program, which is the extension of *MultiSmart3D* coded by the authors' research group (Pan et al. 2007), was generated and numerical results for the isotropic layered half-space were compared with existing ones to demonstrate the accuracy of this method. Also presented are the numerical results for a transversely isotropic layered half-space with examples elucidating clearly the effect of material anisotropy on the pavement response.

GENERAL SOLUTIONS

The transversely isotropic layered half-space is first modeled as in Fig. 1, where the z-axis is positive downward, and the isotropic plane is chosen to be parallel to the horizontal plane. In this model, there are p layers lying on the homogeneous half-space with h_i (i=1, 2... p) being the layer thickness, and H the total thickness above the half-space. The uniform horizontal load acting on the surface z=0. The load configuration is presented in Fig. 2, where X-Y is the global coordinate and P_f is the horizontal projection of the field point z_f. The local coordinate x-y is also chosen with x along the loading direction, and α, β the orientations of the horizontal load and field point to x-axis, respectively.

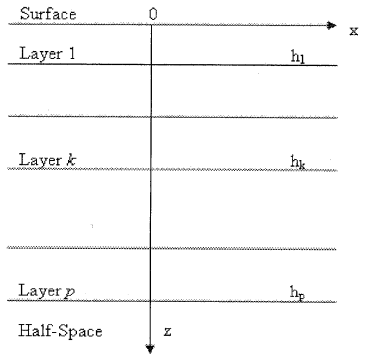

FIG. 1. Geometry of a transversely isotropic multilayered half-space.

By introducing the vector functions in the cylindrical coordinates as in Pan (1989b), the displacement and traction vectors can be expressed as:

$$\boldsymbol{u}(r,\theta,z) = u_{rr}\boldsymbol{r} + u_{\theta\theta}\boldsymbol{\theta} + u_{zz}\boldsymbol{z}$$

$$= \sum_{m} \int_{0}^{+\infty} [U_L(z)\boldsymbol{L}(r,\theta) + U_M(z)\boldsymbol{M}(r,\theta) + U_N(z)\boldsymbol{N}(r,\theta)]\lambda d\lambda \quad (1)$$

$$\begin{aligned}\boldsymbol{t}(r,\theta,z) &= \sigma_{rz}\boldsymbol{r} + \sigma_{\theta z}\boldsymbol{\theta} + \sigma_{zz}\boldsymbol{z} \\ &= \sum_m \int_0^{+\infty} [T_L(z)\boldsymbol{L}(r,\theta) + T_M(z)\boldsymbol{M}(r,\theta) + T_N(z)\boldsymbol{N}(r,\theta)]\lambda d\lambda\end{aligned} \tag{2}$$

where $\boldsymbol{r}$,$\boldsymbol{\theta}$, $\boldsymbol{z}$ are unit vectors along the r-,θ-, z- directions, and

$\boldsymbol{L}(r,\theta;\lambda,m) = \boldsymbol{z}S(r,\theta;\lambda,m)$

$\boldsymbol{M}(r,\theta;\lambda,m) = grad(S) = \boldsymbol{r}\partial S/\partial r + \boldsymbol{\theta}\partial S/(r\partial\theta)$

$\boldsymbol{N}(r,\theta;\lambda,m) = curl(\boldsymbol{z}S) = \boldsymbol{r}\partial S/\partial r - \boldsymbol{\theta}\partial S/(r\partial\theta)$

are vector functions with $S(r,\theta;\lambda,m) = J_m(\lambda r)\exp(im\theta)/(2\pi)^{1/2}$. $J_m(\lambda r)$ is the Bessel function of order m.

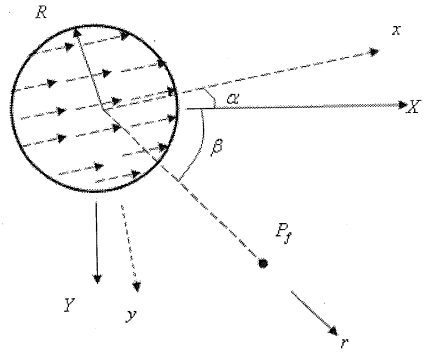

FIG. 2. Geometry of surface loading.

It is noted that for any integrable vector $\boldsymbol{F}$ in the physical domain, its expansion coefficients in the vector function system can be found from the following relations:

$$\begin{aligned}F_L(\lambda,z) &= \frac{2}{\delta_m}\int_0^{2\pi}\int_0^{\infty} \boldsymbol{F}\bullet\boldsymbol{L}^* r dr d\theta \\ F_M(\lambda,z) &= \frac{2}{\delta_m\lambda^2}\int_0^{2\pi}\int_0^{\infty} \boldsymbol{F}\bullet\boldsymbol{M}^* r dr d\theta \\ F_N(\lambda,z) &= \frac{2}{\delta_m\lambda^2}\int_0^{2\pi}\int_0^{\infty} \boldsymbol{F}\bullet\boldsymbol{N}^* r dr d\theta\end{aligned} \tag{3}$$

where:

$$\delta_m = \begin{cases}2 & m=0 \\ 1 & m=1,2,3,...\end{cases}$$

and the vectors $\boldsymbol{L}^*$,$\boldsymbol{M}^*$,$\boldsymbol{N}^*$ are the complex conjugates of $\boldsymbol{L}$,$\boldsymbol{M}$,$\boldsymbol{N}$.

Thus, using the vector functions a relationship between the physical domain $\boldsymbol{F}(r,\theta,z)$ and transformed domain $\boldsymbol{F}_T(\lambda,z)(T=L,M,N)$ is established. Then the physical domain problem can be first solved in the transformed domain, which is more convenient as will be shown below.

After certain manipulation, the solutions in any layer in terms of the vector functions can be obtained

$$\begin{aligned}[E^{LM}(z)]_{4\times1} &= [Z^{LM}(z)]_{4\times4}[K^{LM}]_{4\times1} \\ [E^{N}(z)]_{2\times1} &= [Z^{N}(z)]_{2\times1}[K^{N}]_{2\times1}\end{aligned} \tag{4}$$

where

$$[E^{LM}(z)] = [U_L \quad \lambda U_M \quad T_L/\lambda \quad T_M]^T$$

$$[E^{N}(z)] = [\lambda U_N \quad T_N]^T$$

and the two column matrices $[K]$ are λ-dependent. The expressions for $[Z]$ are listed in Pan (1989b). As can be seen from (4) that, using the vector functions, the coupled 6×6 equations in the physical domain are decoupled into two sets of equations, called LM-type and N-type equations. It should be addressed here that these two sets of equations are independent of each other with a dimension of 4×4 and 2×2, respectively, and thus are computational convenient and efficient.

To solve the multilayered pavement, the propagator matrix method is employed. The propagating relations in the k-th layer with the interfaces z_{k-1} and z_k can be expressed as

$$\begin{aligned}[E^{LM}(z_{k-1})] &= [a_k^{LM}][E^{LM}(z_k)] \\ [E^{N}(z_{k-1})] &= [a_k^{N}][E^{N}(z_k)]\end{aligned} \tag{5}$$

where $[a_k]$ is the propagator matrix and its elements are listed in Pan (1989b). Assuming that the displacement and traction vectors across the layer interface are continuous, solutions for an arbitrary field point can then be expressed as

$$\begin{aligned}[E^{LM}(z)]_{4\times1} &= [G^{LM}(z)]_{4\times4}[K_{p+1}^{LM}]_{4\times1} \\ [E^{N}(z)]_{2\times1} &= [G^{N}(z)]_{2\times4}[K_{p+1}^{N}]_{2\times1}\end{aligned} \tag{6}$$

where $[G(z)]=[a_{fk}][a_{k+1}]\ldots[a_{p-1}][a_p][Z_n(H)]$ with $[a_{fk}]$ being the propagator matrix from field point z_f to the layer interface z_k and $[K_{p+1}]$ being the unknown column matrix in the homogeneous half-space.

In the cylindrical coordinate (Fig. 2), the boundary conditions in the physical domain are

$$\boldsymbol{t}(r,\theta,0) = \sigma_{rz}(r,\theta,0)\boldsymbol{r} + \sigma_{\theta z}(r,\theta,0)\boldsymbol{\theta} + \sigma_{zz}(r,\theta,0)\boldsymbol{z} \tag{7}$$

where for $0\le\theta\le 2\pi$,

$$\begin{aligned}\sigma_{rz}(r,\theta,0) &= q\cos\theta \qquad 0\le r\le R \\ \sigma_{\theta z}(r,\theta,0) &= -q\sin\theta \qquad 0\le r\le R \\ \sigma_{zz}(r,\theta,0) &= 0 \qquad 0\le r<\infty\end{aligned} \tag{8}$$

By virtue of (3), the corresponding boundary conditions in the transformed domain are

$$\begin{aligned}T_L(\lambda,0) &= 0 \\ T_M(\lambda,0) &= \sqrt{2\pi}\frac{qR}{\lambda^2}J_1(R\lambda) \\ T_N(\lambda,0) &= -i\sqrt{2\pi}\frac{qR}{\lambda^2}J_1(R\lambda)\end{aligned} \tag{9}$$

Using the boundary condition on the surface, the solutions in the transformed

domain can be obtained, and then the solutions in physical domain can be arrived. The final solutions are the real part of the following expressions:

$$
\begin{aligned}
u_r(r,\theta,z) &= e^{i\theta}[UT(1)-UT(2)+iUTN(1)]\\
u_\theta(r,\theta,z) &= e^{i\theta}[iUT(2)-UTN(2)+UTN(1)]\\
u_z(r,\theta,z) &= e^{i\theta}[UT(3)]\\
\sigma_{rz}(r,\theta,z) &= e^{i\theta}[UT(4)-UT(5)+iUTN(3)]\\
\sigma_{\theta z}(r,\theta,z) &= e^{i\theta}[iUT(5)-UTN(4)+UTN(3)]\\
\sigma_{zz}(r,\theta,z) &= e^{i\theta}[UT(6)]\\
\sigma_{r\theta}(r,\theta,z) &= e^{i\theta}A_{66}\{UTN(5)+2[UTN(2)-2UTN(1)]/r+2i[UT(1)-2UT(2)]/r\}\\
\sigma_{rr}(r,\theta,z) &= e^{i\theta}\{A_{13}\sigma_{zz}/A_{33}+i(A_{11}-A_{12})[UTN(2)-2UTN(1)]/r\\
&\quad +(A_{13}^2-A_{11}A_{33})UT(7)/A_{33}-(A_{11}-A_{12})[UT(1)-2UT(2)]/r\}\\
\sigma_{\theta\theta}(r,\theta,z) &= e^{i\theta}\{A_{13}\sigma_{zz}/A_{33}-i(A_{11}-A_{12})[UTN(2)-2UTN(1)]/r\\
&\quad +(A_{13}^2-A_{12}A_{33})UT(7)/A_{33}+(A_{11}-A_{12})[UT(1)-2UT(2)]/r\}
\end{aligned}
\tag{10}
$$

where, $UT(i)(i=1,2,\ldots 7)$ and $UTN(i)(i=1,2,\ldots 5)$ are listed in Appendix I. It should be stressed that the UTs are related to LM-type whilst UTNs to N-type.

Based on the above solutions for single loads, coordinate transform is first applied to convert the solutions from local coordinates to global coordinates, and the superposition principle is then employed to derive the final solutions in the global Cartesian coordinates, which are expressed as

$$
\begin{Bmatrix} u_x(P_f)\\ u_x(P_f)\\ u_z(P_f)\end{Bmatrix} = \sum_{i=1}^{N}\left[S^i\right]^T \begin{Bmatrix} u_r(P_f)\\ u_\theta(P_f)\\ u_z(P_f)\end{Bmatrix}^i \tag{11}
$$

for displacements and

$$
\begin{bmatrix} \sigma_{xx} & \sigma_{xy} & \sigma_{xz}\\ & \sigma_{yy} & \sigma_{yz}\\ & & \sigma_{zz}\end{bmatrix} = \sum_{i=1}^{N}\left[S^i\right]^T \begin{bmatrix} \sigma_{rr} & \sigma_{r\theta} & \sigma_{rz}\\ & \sigma_{\theta\theta} & \sigma_{\theta z}\\ & & \sigma_{zz}\end{bmatrix}^i \left[S^i\right] \tag{12}
$$

for stresses with

$$
[S] = \begin{bmatrix} \cos(\beta) & \sin(\beta) & 0\\ -\sin(\beta) & \cos(\beta) & 0\\ & & 1\end{bmatrix}
$$

In (11) and (12), the superscript i means the contribution of the i-th load.

NUMERICAL SOLUTIONS

The solutions in the physical domain using vector functions are in the form of Bessel function integration which requires numerical computation. The infinite integration can be approximated as the summation of partial integration as

$$
\int_0^{+\infty} f(\lambda,z)J_m(\lambda r)d\lambda = \sum_{n=1}^{N}\int_{\lambda_n}^{\lambda_{n+1}} f(\lambda,z)J_m(\lambda r)d\lambda. \tag{13}
$$

The accuracy of the partial integration can be controlled by the pre-chosen error tolerance and satisfactory result can usually be achieved by balancing the time cost and accuracy. In this paper, the error tolerance is fixed at 10^{-4} for the relative error and 10^{-5} for the absolute error. To deal with the possible overflow problem caused by multiplication of propagator matrices, the forward and backward propagating approaches proposed by Pan (1997) and later by Yue and Yin (1998) are also adopted here.

Verification of Results

An example dealing with a three-layered half-space pavement presented in Matsui et al. (2002) is given first to verify the present formulation. The pavement parameters are:

$$
\begin{aligned}
&E_1=2500\text{MPa},\ \nu_1=0.35,\ h_1=0.1\text{m}\\
&E_2=280\text{MPa},\ \nu_2=0.35,\ h_2=0.35\text{m}\\
&E_3=50\text{MPa},\ \nu_3=0.4
\end{aligned}
\tag{14}
$$

In this example, two horizontal loading cases are considered. The first one is a single circular uniform load with Q=49kN and R=0.15m; the second one is double circular uniform loads with $Q_1=Q_2$=49kN, $R_1=R_2$=0.15m, O_1(0,–0.15,0)m, O_2(0,0.15,0)m, $\alpha_1=-\pi/6$, $\alpha_2=\pi/6$, where Q, R, O, α are load magnitude, load radius, load center and load direction, respectively.

Numerical results of displacements and stresses using present formulations and those using BISAR under both single and double horizontal circular loads are presented in Fig. 3 and Fig. 4, respectively. It is clearly observed that present results agree very well with those by BISAR, which therefore provides an indirect verification to our program.

Effect of Horizontal Load

Figs. 5 and 6 show the strain contour of the pavement under vertical and horizontal loads. The horizontal and vertical strains are computed at depth z=0.0999m (within the first layer) and z=0.4501m (within the half-space substrate, i.e., in the third layer), respectively. The pavement structure is still the one used in previous section as in (14). It is evident that the strains under the two kinds of loads are quite different. Under the vertical load in Fig. 5, the strains are symmetric with respect to both x- and y-axes, and ε_{xx} and ε_{yy} are identical to each other after $\pi/2$ rotation. Under the horizontal load in Fig.6, on the other hand, the strains are anti-symmetric with respect to y-axis and symmetric to x-axis. The locations of the maximum strains and the corresponding magnitudes also change greatly. For example, under the same configuration, for the vertical load case the maximum horizontal tensile strains are $\varepsilon_{xx}=3.3\times10^{-4}$, $\varepsilon_{yy}=3.3\times10^{-4}$, and vertical compressive strain is $\varepsilon_{zz}=-7.42\times10^{-4}$, all located at (x,y)=(0,0), whilst under the horizontal load the corresponding strains are $\varepsilon_{xx}=1.33\times10^{-4}$ at about (0.30m,0), $\varepsilon_{yy}=1.36\times10^{-4}$ at about (–0.18m,0), and $\varepsilon_{zz}=-1.34\times10^{-4}$ at (0.25m,0).

Table 1 predicts the effect of the horizontal load on the maximum strains, where b

is the ratio of the horizontal load to vertical load. To predict the fatigue and rutting performance, the following model (Timm and Newcomb, 2006) is used:

$$N_f = 2.83\times10^{-6}\left(\frac{10^6}{\varepsilon_t}\right)^{3.148} \quad (15)$$

$$N_r = 1\times10^{16}\left(\frac{1}{\varepsilon_v}\right)^{3.87} \quad (16)$$

where

N_f = number of cycles until fatigue failure;

N_r = number of cycles until rutting failure;

ε_t = critical horizontal tensile strain at bottom of asphalt layer;

ε_v = critical vertical compressive strain at top of subgrade layer.

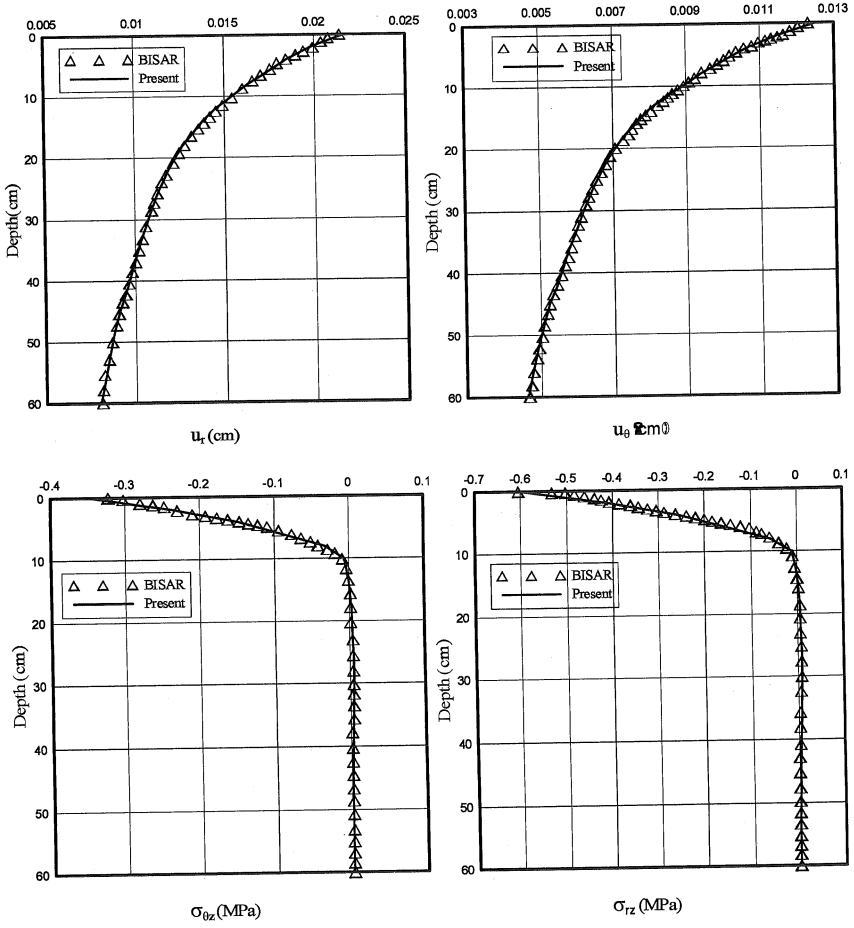

FIG. 3. Comparison of present work and BISAR (single load).

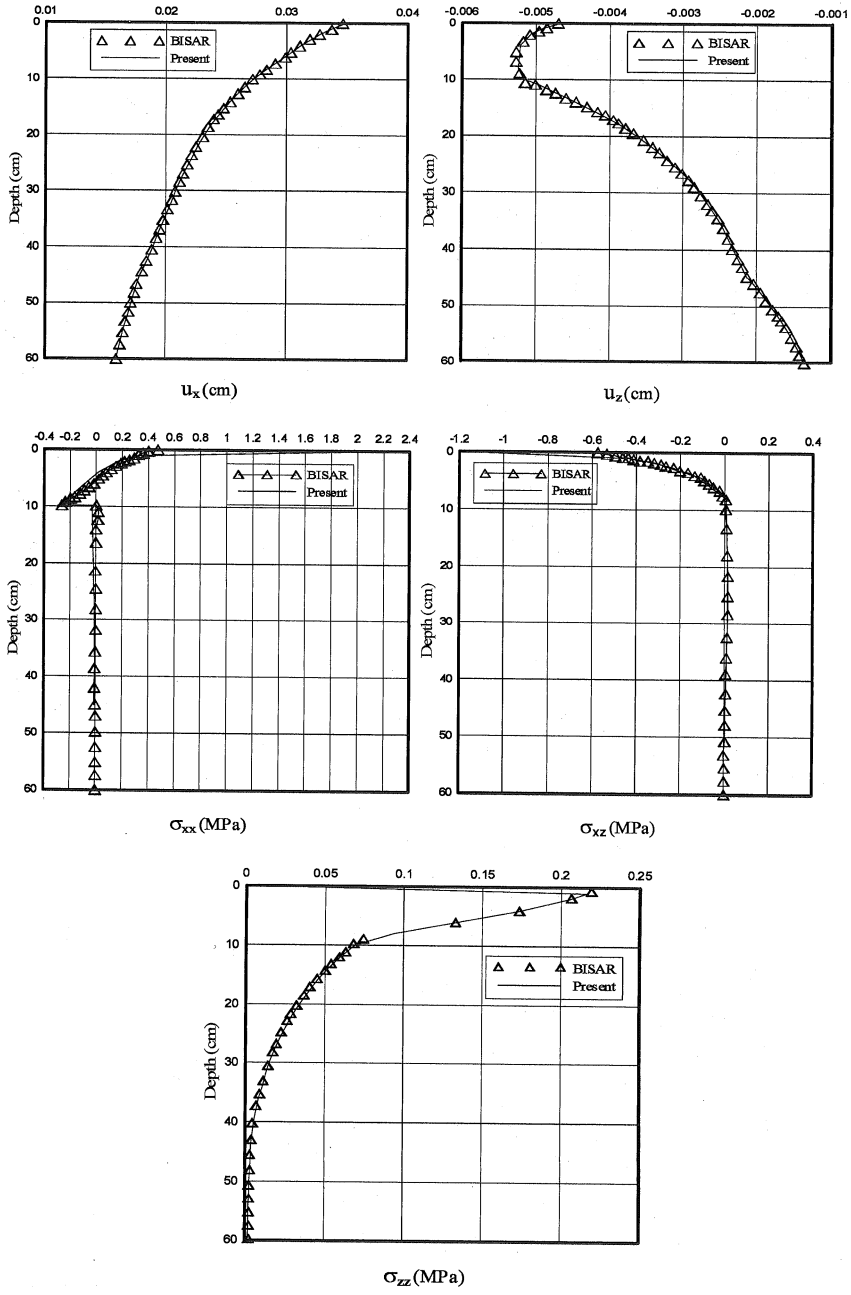

FIG. 4. Comparison of present work and BISAR (double loads).

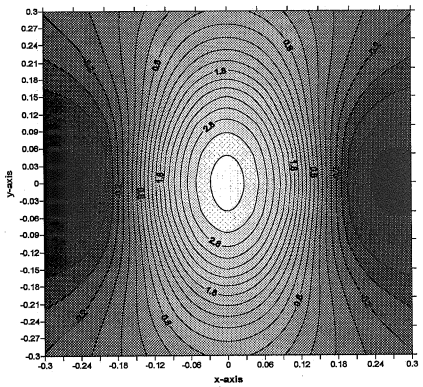

5a. ε_{xx} ($\times 10^{-4}$, at z=0.0999m)

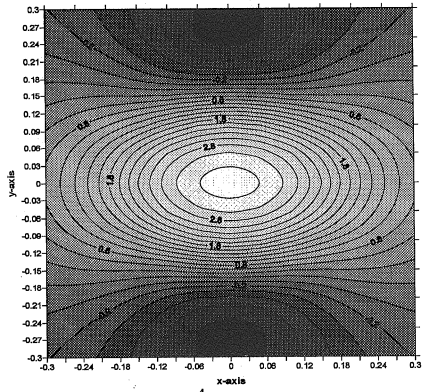

5b. ε_{yy} ($\times 10^{-4}$, at z=0.0999m)

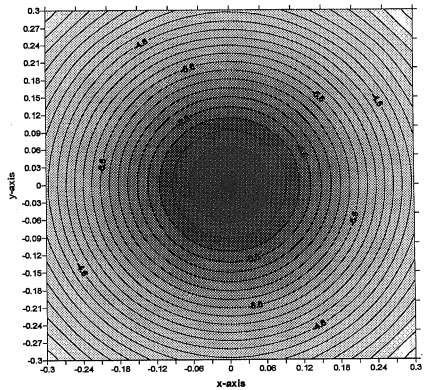

5c. ε_{zz} ($\times 10^{-4}$, at z=0.4501m)

FIG. 5. Vertical loading.

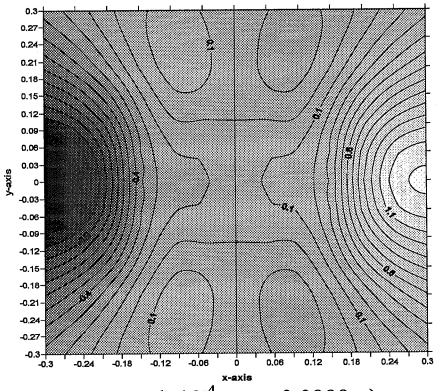

6a. ε_{xx} ($\times 10^{-4}$, at z=0.0999m)

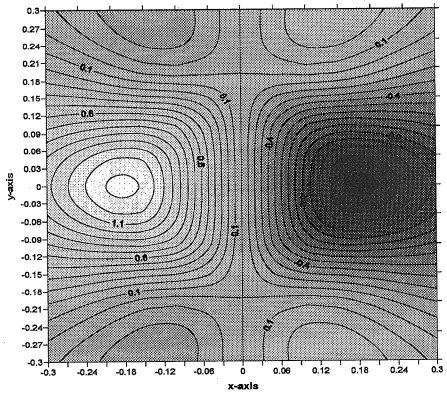

6b. ε_{yy} ($\times 10^{-4}$, at z=0.0999m)

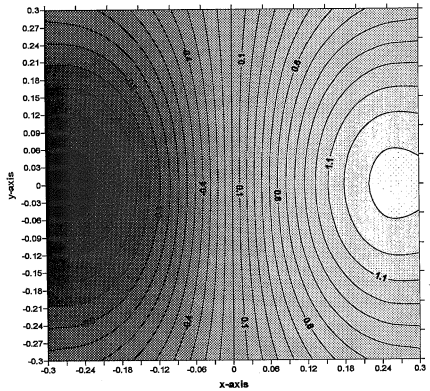

6c. ε_{zz} ($\times 10^{-4}$, at z=0.4501m)

FIG. 6. Horizontal loading.

Table 1. The Effect of Horizontal Load on Fatigue and Rutting Performance

	Fatigue				Rutting	
	ε_{xx} ($\times 10^{-4}$)	ε_{yy} ($\times 10^{-4}$)	ε_t ($\times 10^{-4}$)	N_f($\times 10^{24}$)	ε_v ($\times 10^{-4}$)	N_r($\times 10^{28}$)
b=0	3.3	3.3	3.3	1.9929	-7.4	1.3064
b=0.25	3.4	3.4	3.4	1.8142	-7.6	1.1783
b=1	3.4	4.0	4.0	1.0877	-7.8	1.0660

As can be seen from Table 1, with increasing b, the maximum strains increase, leading to the decrease of N_f and N_r. Thus horizontal load could reduce the fatigue and rutting lifetime. Consequently, ignoring horizontal load would overestimate the failure performance. It also can be observed that the effect of the horizontal load on fatigue is severer than that on rutting. For example, consideration of the horizontal load (e.g. b=1) will reduce a lifetime about 45.42% for fatigue and 18.40% for rutting as compared to the estimation without the horizontal load (e.g. b=0).

Effect of Material Anisotropy

To investigate the effect of pavement anisotropy, Fig. 7 presents the strain contours at depth z=0.0999m for different transversely isotropic pavements (Table 2) under the horizontal load. As mentioned above, the horizontal load would greatly influence fatigue performance which is controlled by the horizontal strain. Thus in Fig. 7 only horizontal strains ε_{xx}, ε_{yy} are presented. It is also noted that for the seven transverse isotropy configurations in Table 2, Case 1 is actually isotropic with the results already being shown in Figs. 6a and 6b. The maximum strains for the seven different cases are also presented in Table 2. The material property definitions in Table 2 are: E and E' are the Young's moduli in the plane of isotropy and in the direction normal to it, respectively; ν and ν' are the Poisson's ratios characterizing the lateral strain responses in the plane of isotropy to a stress acting parallel or normal to it, respectively; G' is the shear modulus in planes normal to the plane of isotropy, and $G=E/2(1+\nu)$. The pavement is again a three-layered structure. However, the material property in each layer is now transversely isotropic. More specifically, the Young's modulus E and Poisson's ratio ν in the first, second and third layers are the same as those listed in (14), and the corresponding $E'$and ν' in each layer are determined using Table 2 for different cases.

Table 2. The Effect of Anisotropy on Fatigue

	E/E'	G/G'	ν/ν'	ε_{xx} ($\times 10^{-4}$)	ε_{yy} ($\times 10^{-4}$)	ε_t ($\times 10^{-4}$)
Case 1	1.0	1.0	1.0	1.4	1.4	1.4
Case 2	1.0	2.0	1.0	1.2	1.3	1.3
Case 3	1.0	3.0	1.0	1.0	1.2	1.2
Case 4	1.5	1.0	1.0	1.3	1.5	1.5
Case 5	3.0	1.0	1.0	1.2	1.8	1.8
Case 6	1.0	1.0	0.75	1.4	1.4	1.4
Case 7	1.0	1.0	1.5	1.4	1.3	1.4

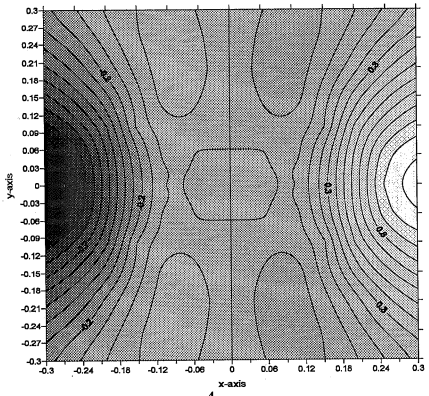

7a. ε_{xx} ($\times 10^{-4}$) Case 2.

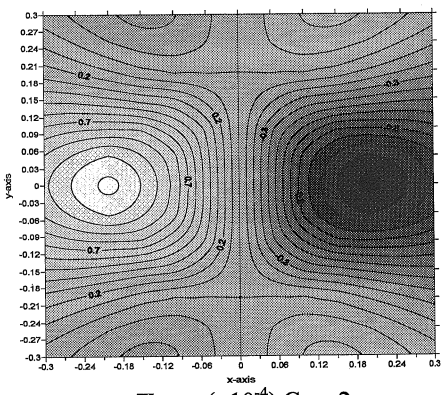

7b. ε_{yy} ($\times 10^{-4}$) Case 2.

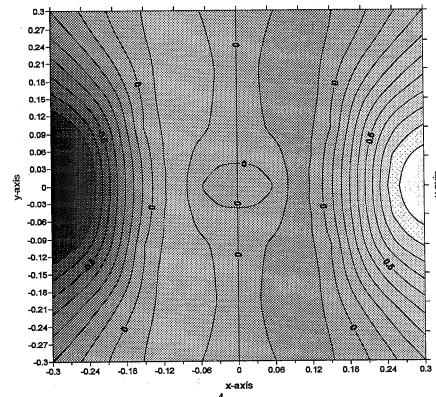

7c. ε_{xx} ($\times 10^{-4}$) Case 3.

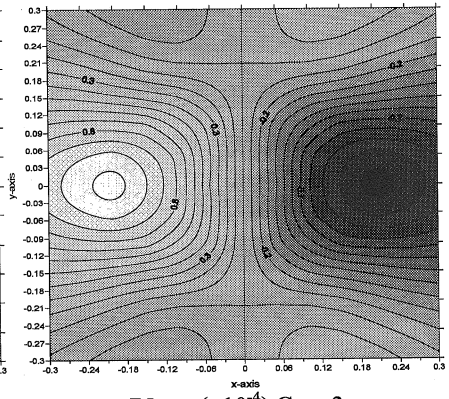

7d. ε_{yy} ($\times 10^{-4}$) Case 3.

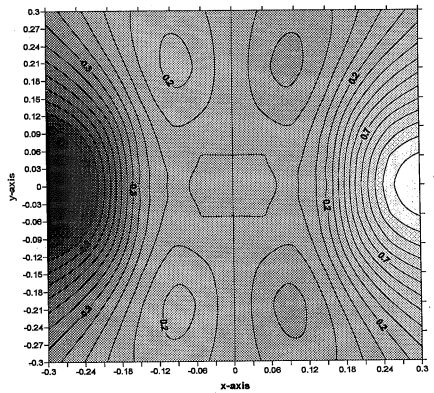

7e. ε_{xx} ($\times 10^{-4}$) Case 4.

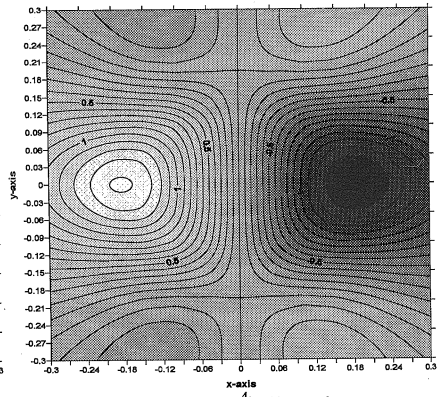

7f. ε_{yy} ($\times 10^{-4}$) Case 4.

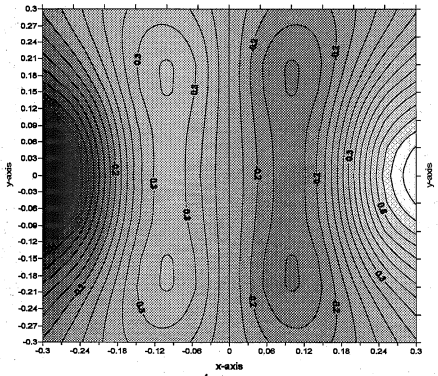

7g. ε_{xx} ($\times 10^{-4}$) Case 5.

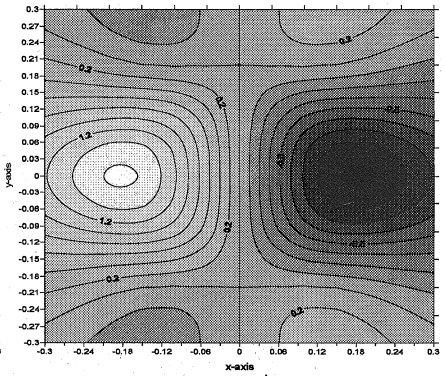

7h. ε_{yy} ($\times 10^{-4}$) Case 5.

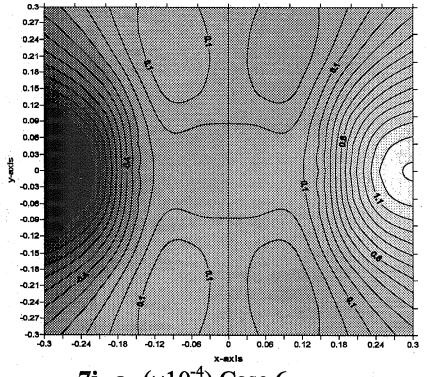

7i. ε_{xx} ($\times 10^{-4}$) Case 6.

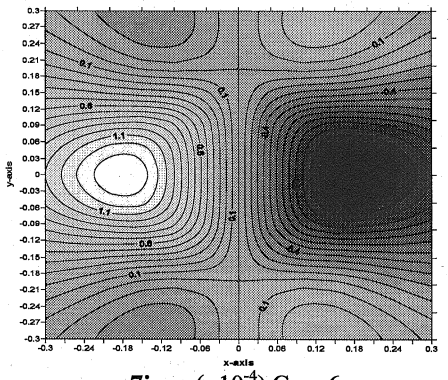

7j. ε_{yy} ($\times 10^{-4}$) Case 6.

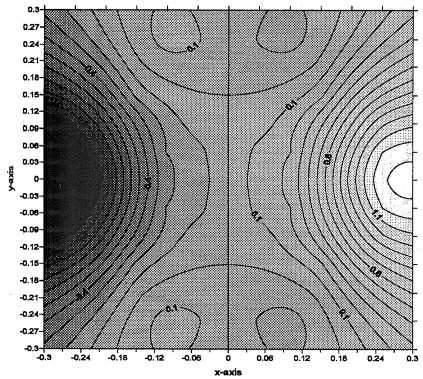

7k. ε_{xx} ($\times 10^{-4}$) Case 7.

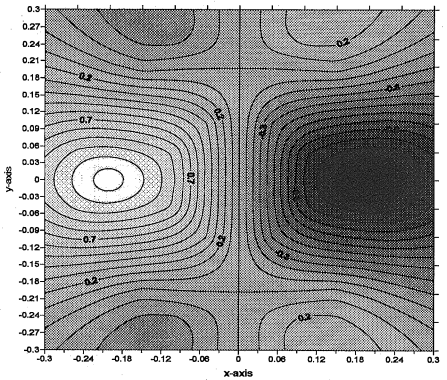

7l. ε_{yy} ($\times 10^{-4}$) Case 7.

FIG. 7. Effect of anisotropy on horizontal strain.

For Cases 1, 2 and 3, it can be seen that with decreasing G', the maximum strain decreases. It is interesting to observe that the maximum strains are all reached by ε_{yy}. Cases 1, 4 and 5 show that maximum strain increases with decreasing E', and the increase is more apparent than the decrease shown in Cases 1, 2 and 3. Thus the strains are more sensitive to E' than to G'. Similarly, the maximum strains are also reached by ε_{yy}. From Cases 1, 6 and 7 it is easy to conclude that the maximum strain slightly decreases with decreasing ν' and are reached by ε_{xx}.

It is also interesting to find that the maxima ε_{xx} for all the seven cases are located within the domain $x\in(0.24\text{m}, 0.36\text{m})$ and $y\in(-0.06\text{m}, 0.06\text{m})$, whilst for the maxima ε_{yy} they are in the domain $x\in(-0.24\text{m}, -0.12\text{m})$ and $y\in(-0.06\text{m}, 0.06\text{m})$, although their magnitudes are different. It can be anticipated that under the same horizontal load configuration the critical strains will always be in the same domains without being affected by the anisotropy configuration.

CONCLUSIONS

In this work, the response of a layered half-space pavement to multiple horizontal loads acting on the surface is established, and a FORTRAN program is developed based on the present solution. The effect of the horizontal load is then discussed showing that the horizontal load has a great influence on the pavement fatigue performance. For example our results show that ignoring the horizontal load would result in an overestimate on the lifetime expectance of the pavement. Further discussed in this paper is the effect of the pavement anisotropy on the strains, showing that the critical strains are mostly sensitive to E, then to G and less to ν. The anisotropy will change greatly the magnitude of the critical strain but slightly its position. Thus to predict the failure performance in pavement engineering, it is anticipated that only certain domains, rather than the whole field, need to be computed, which will greatly reduce the computation time.

APPENDIX

$$UT(1)=\int_0^\infty(\lambda U_M/\lambda)J_0(\lambda r)\lambda^2 d\lambda \qquad UT(4)=\int_0^\infty(T_M)J_0(\lambda r)\lambda^2 d\lambda$$

$$UT(2)=\int_0^\infty(\lambda U_M/\lambda^2 r)J_1(\lambda r)\lambda^2 d\lambda \qquad UT(5)=\int_0^\infty(T_M/r)J_1(\lambda r)\lambda d\lambda=\int_0^\infty(T_M/\lambda r)J_1(\lambda r)\lambda^2 d\lambda$$

$$UT(3)=\int_0^\infty U_L J_1(\lambda r)\lambda d\lambda=\int_0^\infty(U_L/\lambda)J_1(\lambda r)\lambda^2 d\lambda \quad UT(6)=\int_0^\infty T_L J_1(\lambda r)\lambda d\lambda=\int_0^\infty(T_L/\lambda)J_1(\lambda r)\lambda^2 d\lambda$$

$$UT(7)=\int_0^\infty U_M\lambda^2 J_1(\lambda r)\lambda d\lambda=\int_0^\infty(\lambda U_M)J_1(\lambda r)\lambda^2 d\lambda$$

$$UTN(1)=\int_0^\infty(\lambda U_N/\lambda^2 r)J_1(\lambda r)\lambda^2 d\lambda \qquad UTN(2)=\int_0^\infty(\lambda U_N/\lambda)J_0(\lambda r)\lambda^2 d\lambda$$

$$UTN(3)=\int_0^\infty(T_N/r)J_1(\lambda r)\lambda d\lambda=\int_0^\infty(T_N/\lambda r)J_1(\lambda r)\lambda^2 d\lambda$$

$$UTN(4)=\int_0^\infty(T_N)J_0(\lambda r)\lambda^2 d\lambda$$

$$UTN(5)=\int_0^\infty U_N\lambda^2 J_1(\lambda r)\lambda d\lambda=\int_0^\infty(\lambda U_N)J_1(\lambda r)\lambda^2 d\lambda$$

REFERENCES

Burmister, D.M. (1943). "The theory of stresses and displacements in layered systems and applications to the design of airport runways." *Proc. Hwy. Res. Board*, Vol. 23: 126-144.

Burmister, D.M. (1945). "The general theory of stresses and displacements in layered soil systems." *J. Appl. Phys.*, Vol. 16: 89-94, 126-127, 296-302.

Love, A.E.H. (1927). A treatise on the mathematical theory of elasticity, Cambridge University, fourth edition.

Matsui, K., Maina, J. W., Dong, Q., and Inoue, T. (2002). "Development of pavement structural analysis due to horizontal surface force based on elastic theory." *Proc., the 2002 FAA Airport Technology Transfer Conference*, P-37, Atlantic City, New Jersey.

Mindlin, R. D. (1936). "Force at a point in the interior of a semi-infinite solid." *J. Appl. Phys.*, Vol. 7: 195-202.

Pan, E. (1989a). "The static responses of multilayered foundations to general surface loading and body force." *Acta. Mech. Sin.*, 21(3): 344-353 (in Chinese).

Pan, E. (1989b). "Static response of a transversely isotropic and layered half-space to general surface loads". *Phys. Earth Planet. Inter.*, Vol.54: 353-363.

Pan, E. (1997). "Static Ggreen's functions in multilayered half-spaces." *Appl. Math. Modell.*, Vol.21: 509-521.

Pan, E., Alkasawneh, W., and Chen, E. (2007). "An exploratory study on functionally graded materials with application to multilayered pavement design." *Report* FHWA/OH-2007/12, Ohio Department of Transportation, Columbus, Ohio.

Timm, D.H. and Newcomb, D.E. (2006). "Perpetual pavement design for flexible pavements in the U.S." *Int. J. of Pavement Engineering*, 7(2): 111-119.

Wang, K. (1983). "Calculation of stresses, strains and displacements in an *N*-layer elastic continuous system under the action of two complex loads uniformly distributed on circular areas." *Acta. Mech. Sol. Sin.*, Vol.1: 136-153 (in Chinese).

Wardle, L.J. (1981). "Three-dimensional solution for displacement discontinuities in cross- anisotropic elastic media." *CSIRO Aust. Div. Appl. Geomech. Tech. Pap.*, Vol.34: 1-32.

Yue, Z.Q. and Yin, J.H. (1998). "Backward transfer-matrix method for elastic analysis of layered solids with imperfect bonding." *J. Elasticity*, Vol.50: 109-128.